Journal of the Ceramic Society of Japan 116 [4] 566-571 2008 Paper

Effects of adding Y_2O_3 on the electrical resistivity of aluminum nitride ceramics

Hiroaki SAKAI,[*] Yuji KATSUDA,[*] Masaaki MASUDA,[*] Chikashi IHARA[*] and Tetsuya KAMEYAMA[,***]**

[*]NGK Insulators, Ltd., 2–56 Suda-cho, Mizuho-ku, Nagoya 467–8530
[**]Environmental Technology and Urban Planning, Nagoya Institute of Technology, Gokiso-cho, Showa-ku, Nagoya 466–8555
[***]National Institute of Advanced Industrial Science and Technology (AIST), 2266–98, Anagahora, Shimoshidami, Moriyama-ku, Nagoya 463–8560

Electrical resistivity of AlN ceramics was examined with various amounts of Y_2O_3 within 0 to 4.8 mass%. The electrical resistivity at room temperature varied from 10^{16} to 10^{10} Ω·cm with different Y_2O_3 amounts and at sintering temperatures. In the typical samples sintered at 1900°C, a smaller amount of Y_2O_3 addition with 0.1 to 0.5 mass% gives the lowest electrical resistivity of 10^{10} Ω·cm, whereas the higher amount of Y_2O_3 maintains high resistivity of more than 10^{13} Ω·cm. The results derived from different analytical techniques such as impedance analysis, cathodoluminescence spectrum and microstructural analysis explain the importance of the oxygen concentration in the AlN grain for the electrical resistivity of AlN ceramics.

Key-word : Aluminum nitride, Yttria, Electrical resistivity, Impedance analysis, Cathodoluminescence, Microstructure

[Received November 8, 2007; Accepted February 21, 2008]

1. Introduction

Aluminum nitride (AlN) has a high thermal conductivity, high corrosion resistivity, and a similar thermal expansion to silicon. Therefore, the sintered AlN ceramics are used for electronic substrates, heat sinks, and semiconductor producing components.[1)–5)] In addition to the above mentioned characteristics, it is very important to control the electrical resistivity of AlN ceramics when they are used for such electronic applications. For example, electronic substrates require high electrical resistivity to ensure high insulation. In the application for semiconductor producing components such as electrostatic chucks, the electrical resistivity must be kept within the proper range.[5)]

Generally, sintering additives promoting the liquid phase sintering are used for the densification of AlN ceramics. The typical sintering additives are rare-earth oxides such as Y_2O_3. During sintering, Y_2O_3 reacts with the oxygen impurity of AlN powder forming yttrium-aluminates second phases. The formations of such second phases are useful not only to promote liquid phase sintering, but also to improve the thermal conductivity due to the reduction of phonon scattering in the AlN grain by oxygen defects.[6),7)]

As for the electrical resistivity or conductivity behavior of AlN ceramics, there are a few reports published so far. For example, Richards et al. investigated the electrical conductivity of BeO doped hot-pressed AlN ceramics as a function of temperature from 800 to 1200°C within different nitrogen partial pressures.[8)] They reported that the conductivity is independent of the nitrogen partial pressure and decreases with beryllium doping. The charge carriers are concluded to be either extrinsic electrons or aluminum vacancies. Yahagi et al. measured the ionic conduction of Y_2O_3 or Al_2O_3 doped AlN ceramics at temperatures of 900 to 1500°C by using the d-c polarization and the electromotive force measurement.[9)] They considered that Al^{3+} ions are charge carriers for the electrical conduction. Groen et al. performed the complex impedance analysis on several AlN ceramics at high temperatures of 575 to 1100°C.[10)] They indicated that the calculated activation energy of 2.1 eV for the electrical conduction of bulk AlN grains agreed well with the ionization energy for the oxygen defect in AlN. Therefore, the ionization of the oxygen defect is considered to be the charge generating reaction. More recently, Yoshikawa et al. reported the room-temperature electrical resistivity of Sm_2O_3 doped AlN ceramics by using a DC three-pole method.[11)] They disclosed that the three-dimensional network of grain boundary phase consisting of Sm-β-alumina decreases the electrical resistivity of AlN ceramics from more than 10^{14} to 10^{10} Ω·cm.

In this paper, the electrical resistivity behavior of AlN ceramics with different amounts of Y_2O_3 is investigated. The observed electrical resistivity is discussed in combination with other characteristics determined by thermal analysis, microstructural observation, XRD analysis and so on.

2. Experimental

2.1 Sample preparation

A high purity AlN powder, which is available commercially (Tokuyama, F-Grade), was used as the starting material. The oxygen content was 0.9 mass%. The total metal element impurities were less than 30 ppm and the carbon content was 300 ppm. The amount of Y_2O_3 added to the AlN powder was 0.1, 0.3, 0.5, 1.0, 2.9 and 4.8 mass%. In order to obtain homogeneous composition in powder mixtures, $Y(NO_3)_3 \cdot 6H_2O$, which is soluble in isopropyl alcohol, was used as the Y_2O_3 source when the amount was within 0.1 and 0.5 mass%. High purity Y_2O_3 powder (Shin-Etsu Chemical Co., Ltd., RU-Grade) was used when the amount was over 1.0 mass%. Isopropyl alcohol was used as the solvent for wet mixing with conventional ball-mill. After the wet mixing, the mixture was dried and granulated by sieving. The mixture was then shaped into a disk by using uniaxial pressing. The diameter and thickness of the disk were 100 mm and 20 mm, respectively. The disk was placed in a graphite die and hot-

pressed in a nitrogen atmosphere. The sintering temperature was between 1700 to 2000°C and the holding time was four hours. It was confirmed that the obtained sintered bodies reached the theoretical density for each composition.

2.2 Characterization

The volume resistivity of the sintered AlN samples was measured by using a DC three-pole method (JIS C2141). Measurements were taken in a normal air atmosphere at room temperature and in a vacuum at high-temperature. The shape of the test sample had a diameter of 50 mm and a thickness of 1 mm. The diameter of the main electrode was 20 mm, the inner diameter of the guard electrode was 30 mm and the diameter of the power-applying electrode was 40 mm. The applied voltage was fixed at 500 V/mm. The volume resistivity was calculated based on the current value one minute after the power supply. An impedance analyzer was also used to separate the resistance components of the representative samples.

The crystal phase was analyzed by an X-ray diffractmeter (XRD) with CuKα radiation. The lattice parameter was calculated by using the whole powder pattern decomposition (WPPD) method. The microstructure was observed using a scanning electron microscope (SEM). Electron probe microanalysis (EPMA) was also carried out for the analysis of elemental distribution. Lattice defects were evaluated with cathodoluminescence spectroscopy equipped in the SEM. The laser flash method (JISR1611) was used for the thermal conductivity measurements.

3. Results

3.1 Volume resistivity at room temperature

Figure 1 shows the room-temperature volume resistivity of AlN ceramics sintered with different amounts of Y_2O_3 and at different sintering temperatures. It was found that the higher the sintering temperature, the lower the volume resistivity in the same compositions. As for the effect of the amount of Y_2O_3, once the volume resistivity decreased with increasing the Y_2O_3 amount, then the resistivity became higher than the AlN without Y_2O_3. These behaviors were more obvious at sintering temperatures over 1900°C. When the Y_2O_3 amount was 0.3 mass%, the volume resistivity had a minimum value of 10^{10} Ω·cm at room temperature.

3.2 Volume resistivity at high temperatures

Figure 2 shows the temperature dependency of the volume

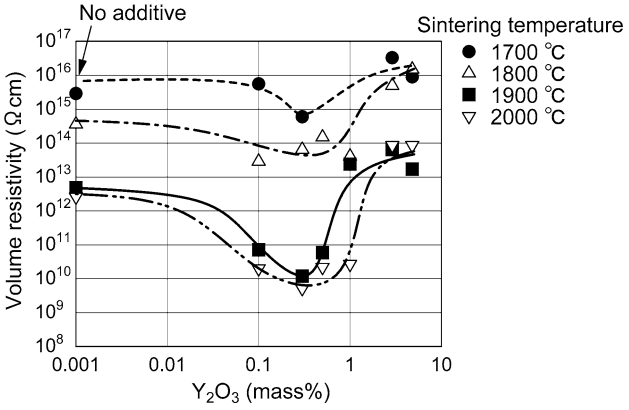

Fig. 1. Room-temperature volume resistivity of the AlN ceramics sintered with different amounts of Y_2O_3 and at different sintering temperatures.

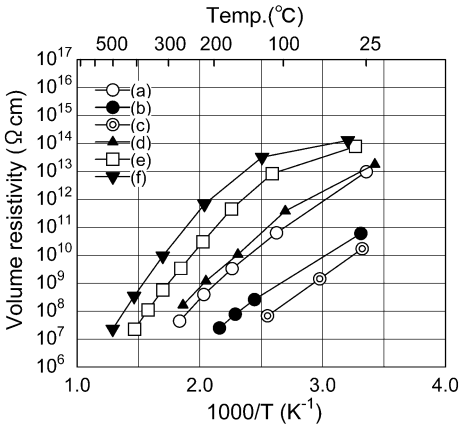

Fig. 2. Arrhenius plots for the volume resistivity of AlN ceramics sintered at 1900°C. The Y_2O_3 amounts are (a) 0 mass%, (b) 0.1 mass%, (c) 0.3 mass%, (d) 1.0 mass%, (e) 2.9 mass% and (f) 4.8 mass%, respectively.

was 2.9 and 4.8 mass%, which showed higher resistivity at room temperature, the curves bent between 140 to 160°C. The activation energy of them at high temperatures was about 1.1 to 1.2 eV. On the other hand, in the samples having lower resistivity of less than 10^{11} Ω·cm at room temperature, the curves showed no bend with the activation energy of around 0.6 eV. In the mean resistivity of 10^{13} Ω·cm for AlN with 0 and 1.0 mass% Y_2O_3, the curves bent slightly between 100 to 110°C. The activation energy at high temperatures was 0.8 eV. These differences in the activation energy indicate that the conduction controlling mechanisms are different among the samples.

3.3 Resistance analysis using the AC impedance method

The AC impedance analysis was applied to separate the resistance components of the representative AlN samples sintered at 1900°C. **Figure 3** shows the Cole–Cole plots obtained from this analysis. There were two semicircles observed in the samples without and with 0.3 mass% Y_2O_3. It indicates that these samples have two different resistance components. That is, the lower resistivity of both samples was calculated to be about 10^8 Ω·cm from the x-intercept. On the other hand, their higher resistivity components had difference in two orders of magnitudes, where the sample without Y_2O_3 was 10^{12} and the other one with 0.3 mass% Y_2O_3 was 10^{10} Ω·cm. The sample with 2.9 mass% Y_2O_3, which had a higher resistivity, only exhibited the rising portion of the first semicircle due to the measurement limitation. This result revealed that their resistivity components were over 10^{13} Ω·cm.

3.4 Crystal phase analysis

The sintering additives remaining in the matrix are possible to affect the electrical resistivity. Therefore, the second phases for each sample were analyzed by an XRD. **Figure 4** shows the XRD diagrams of the samples sintered at 1900°C. In the AlN sample without Y_2O_3, (a), Al_5O_6N was identified except AlN. The representative peaks belonging to Al_5O_6N are denoted by open circles (○). It was considered that the Al_5O_6N was formed by the reaction between AlN and oxygen impurity in the raw AlN powder. When the amount of Y_2O_3 was within 0.1 to 0.5 mass%, $Y_3Al_5O_{12}$ (△) was identified along with the Al_5O_6N. By increasing the Y_2O_3 amount, only $Y_3Al_5O_{12}$ peaks appeared in

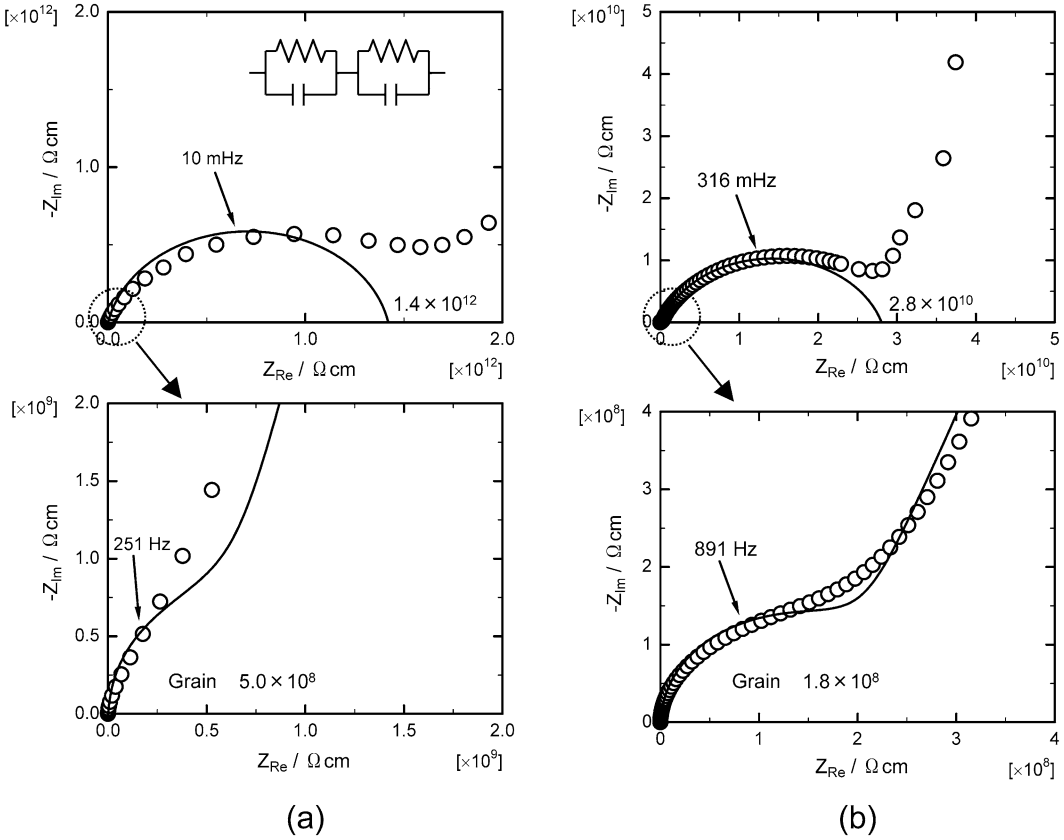

Fig. 3. Cole–Cole plots for the AlN ceramics, (a) without Y_2O_3 and (b) with 0.3 mass% Y_2O_3.

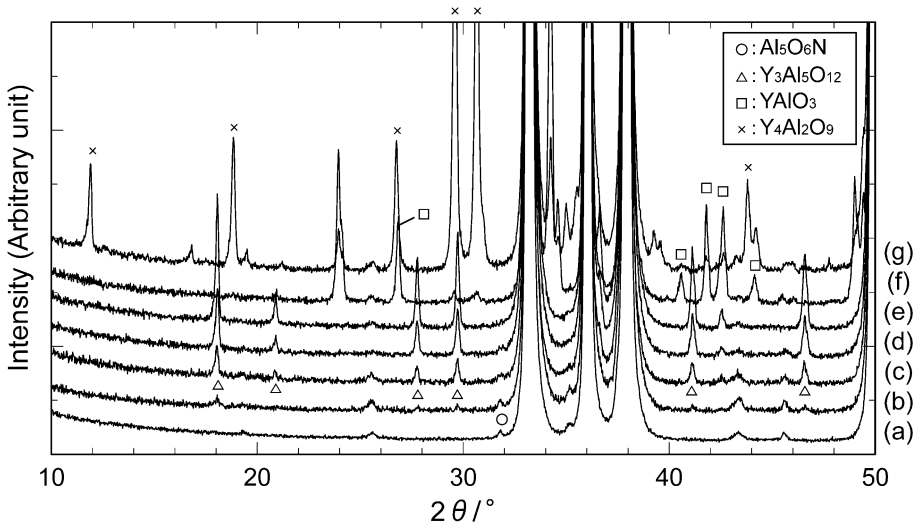

Fig. 4. XRD diagrams of the AlN ceramics sintered at 1900°C. The Y_2O_3 amounts are (a) 0 mass%, (b) 0.1 mass%, (c) 0.3 mass%, (d) 0.5 mass%, (e) 1.0 mass%, (f) 2.9 mass%, and (g) 4.8 mass%. Marks denote representative peak positions of the secondary phases.

the AlN with 1.0 mass% Y_2O_3. A further increase of Y_2O_3 to 2.9 and 4.8 mass% remained $YAlO_3$ (□) and $Y_4Al_2O_9$ (×) in the AlN. It was determined that observed second phases were in good coincidence with the crystal phases estimated from the binary phase diagram of the Al_2O_3 and Y_2O_3,[12] where the oxygen impurity in the AlN powder was considered to be Al_2O_3.

3.5 Microstructural analysis

Figure 5 shows the backscattered SEM images of the polished AlN samples sintered at 1900°C. The size of AlN grains without Y_2O_3, (a), smaller than Y_2O_3 added ones, (b) and (c), with their edge relatively jagged. On the other hand, the AlN grains with Y_2O_3 had a tendency to be hexagonal and uniform in shape with a larger size. Comparing the results derived from the XRD of Fig. 4, it can be mentioned that the second phase observed as bright portions in Fig. 5 are mainly $Y_3Al_5O_{12}$ for 0.3 mass%, $YAlO_3$ for 2.9 mass% and $Y_4Al_2O_9$ for 4.8 mass% Y_2O_3 doped AlN. It was also observed by the fracture surface analysis by

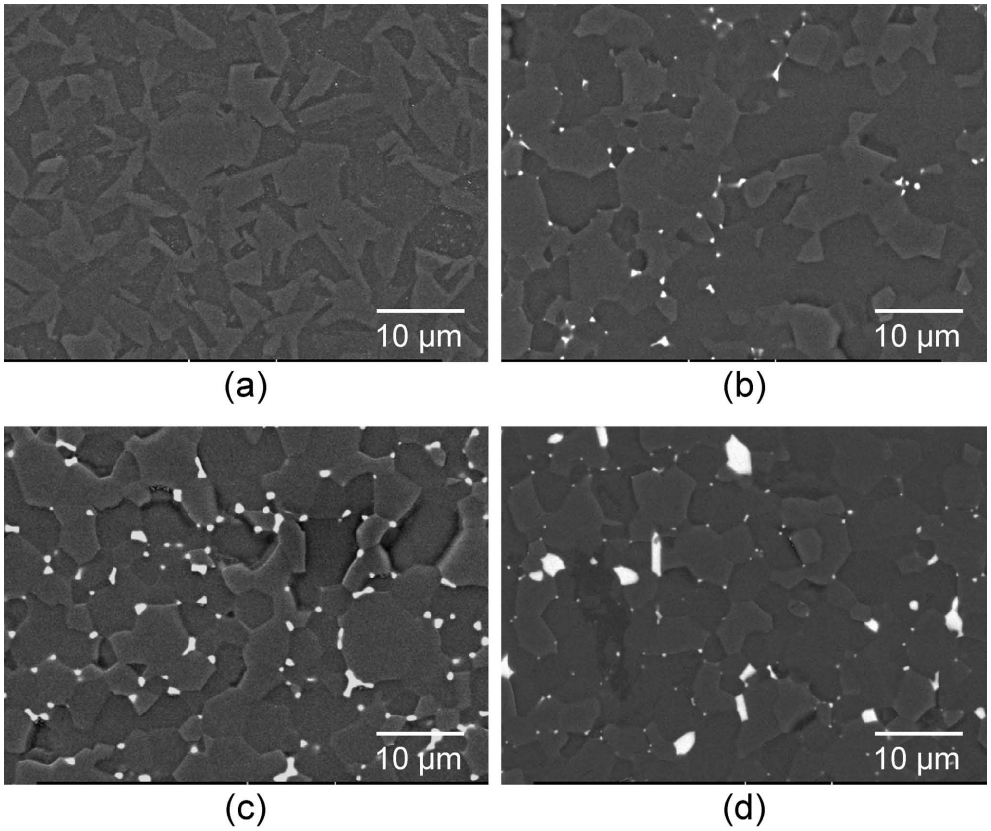

Fig. 5. Backscattered scanning electron images of the polished AlN ceramics sintered at 1900°C. The Y_2O_3 amounts are (a) 0 mass%, (b) 0.3 mass%, (c) 2.9 mass% and (d) 4.8 mass%.

SEM that the sample without Y_2O_3 had the transgranular fracture in majority; however, it turned to be intergranular in Y_2O_3 doped AlN.

Figure 6 shows the electron probe microanalysis (EPMA) images of the polished AlN ceramics sintered at 1900°C. The results were obtained from the samples without additive, (a), with 0.3 mass%, (b), and 2.9 mass% Y_2O_3, (c), respectively. As shown in the center images of the sample with no additive, (a), the isolated oxygen portion about 5 μm were corresponding to be Al_5O_6N. As for the AlN with 0.3 mass% Y_2O_3, it was found that there were two different portions in oxygen and yttrium distribution: the one which had only oxygen corresponded to Al_5O_6N, as in the same with no additive, and the other where both oxygen and yttrium existed together coincided with $Y_3Al_5O_{12}$. In the case of the AlN with 2.9 mass% Y_2O_3, the oxygen and yttrium distributions were mainly corresponding to $YAlO_3$. According to the microstructural analysis shown in Fig. 5 and 6, the second phase of each sample was isolated like islands. This indicated that the continuous second phase derived by wetting at the grain boundary did not occur in these samples. As for the oxygen concentration in the AlN matrix, it can be considered that the color difference of oxygen is proportional to the amount of dissolved oxygen in the AlN grain. From the observed images shown in Fig. 6, the amount of dissolved oxygen in the AlN grain was decreasing with increasing the Y_2O_3 amount from 0 mass%, 0.3 mass% to 2.9 mass% Y_2O_3. Therefore, it can be noted that the amount of oxygen concentration in the AlN grain depends on the amount of the added Y_2O_3.

3.6 Cathodoluminescence spectrum

The cathodoluminescence spectrum of the AlN samples was measured to analyze the impurity level in the AlN bandgap. From the results shown in **Fig. 7**, the wide luminescence spectrum around 370 nm was observed in the both samples without and with 0.3 mass% Y_2O_3. On the other hand, in the sample with 2.9mass% Y_2O_3, almost no luminescence could be obtained. The spectrum at 370 nm is equivalent to 3.4 eV, which is about a half of the AlN bandgap of 6.2 eV.

4. Discussion

Table 1 shows the summary of the results so far obtained from the AlN ceramics with 0 mass%, 0.3 mass% and 2.9 mass% Y_2O_3 sintered at 1900°C. In this table, the measured lattice parameter and oxygen concentration in the AlN grain, which was calculated by using the Slack's equation[13] and the measured thermal conductivity are also listed. The c-axis lattice constant had a tendency to increase with an increase of the Y_2O_3 amount and their thermal conductivity. The calculated oxygen concentrations were 10.2×10^{20} atom/cm^3 and 7.8×10^{20} atom/cm^3 for the samples without and with 0.3 mass% Y_2O_3. However, in the sample with 2.9 mass% Y_2O_3, the number 2.7×10^{20} atom/cm^3 is only a third of other samples. These tendencies were in good agreement with the observed oxygen concentration of AlN matrix by EPMA. Moreover, considering the cathodoluminescence spectrum, where a higher oxygen concentration in the AlN gave the peak at 370 nm and no peaks observed in the AlN with a low oxygen concentration, and major impurity of oxygen in the AlN raw powder, it can be concluded that the cathodoluminescence spectrum at 370 nm is emitted from the oxygen impurity

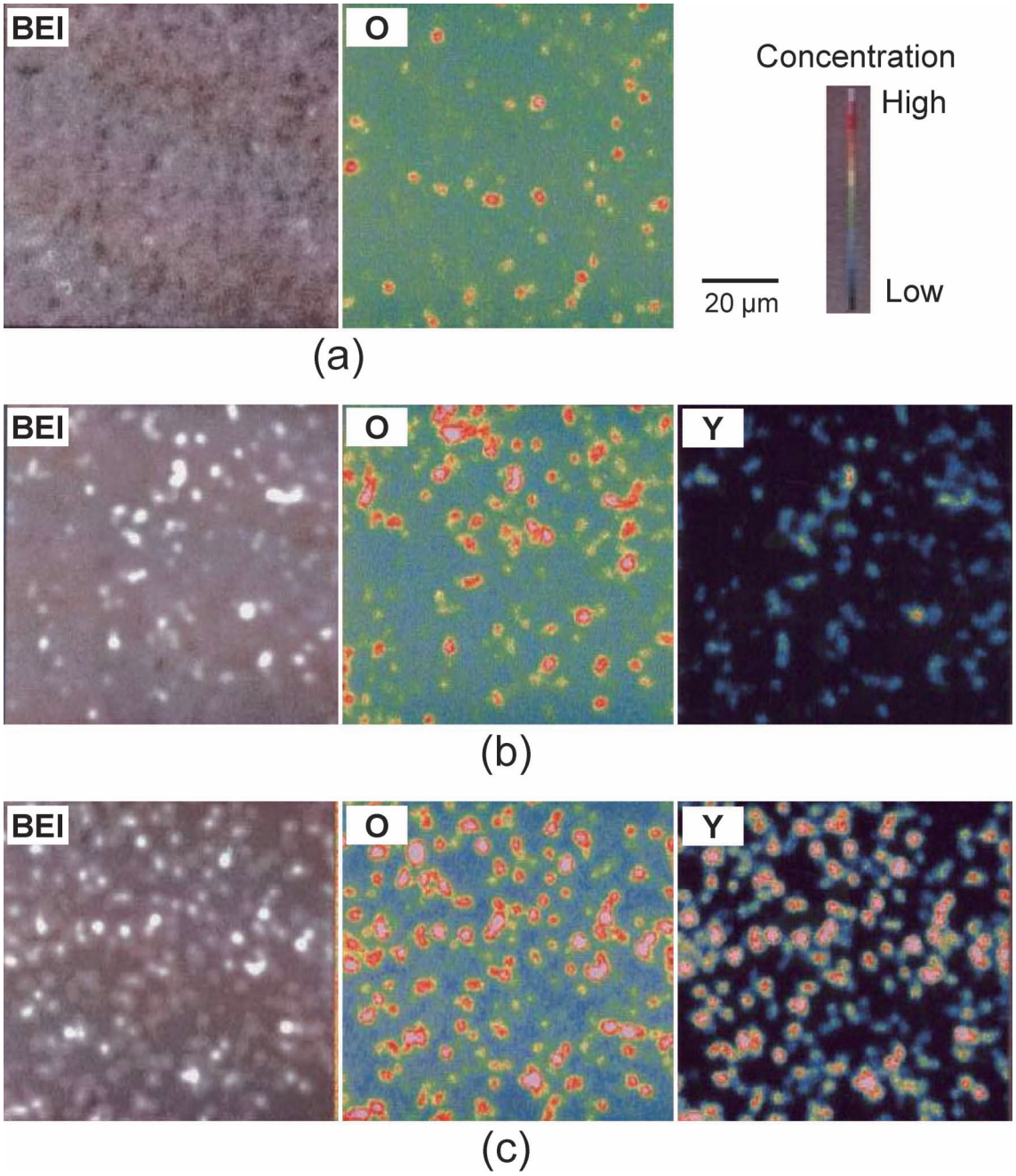

Fig. 6. Electron probe microanalysis images of the polished AlN ceramics sintered at 1900°C. The Y_2O_3 amounts are (a) 0 mass%, (b) 0.3 mass% and (c) 2.9 mass%. The left, center, and right images correspond to the backscattered scanning electron images, oxygen mappings, and yttrium mappings, respectively.

level in the AlN grain.

The above-mentioned microstructural characteristics of AlN and the resistance components determined by impedance analysis can suggest the following mechanisms. Generally, the constituents of the resistance component for polycrystalline ceramics are divided into the grain and grain boundary resistances. In some cases, the existence of a second phase can be critical when they form network structures in the matrix. But this is not the case for this study as shown in Fig. 5. Therefore, it can be considered that lower resistance components of the AlN samples without and with 0.3 mass% Y_2O_3 is corresponding to the grain resistivity. That is, the conductive carriers are introduced in the AlN due to the oxygen dissolution. On the other hand, in the sample having a low oxygen concentration as revealed in the AlN with 2.9 mass% Y_2O_3, the oxygen impurities are removed from the AlN grain during sintering by the reaction between adding the Y_2O_3 and oxygen component in the AlN raw powder. Therefore, the oxygen trapped by Y_2O_3 is critical not only for the thermal conductivity, as mentioned in much of the literature in this subject,[1),6),7),11)] but also the grain resistivity. It is also considered that the incorporation of oxygen into the nitrogen site in an AlN lattice generates the electrons for the dominant charge carriers. The difference in the grain boundary resistivity between the sample without Y_2O_3 and 0.3 mass% Y_2O_3 can be explained in terms of the differences in the grain size. The smaller grain size of no additives gives the higher number of apparent grain

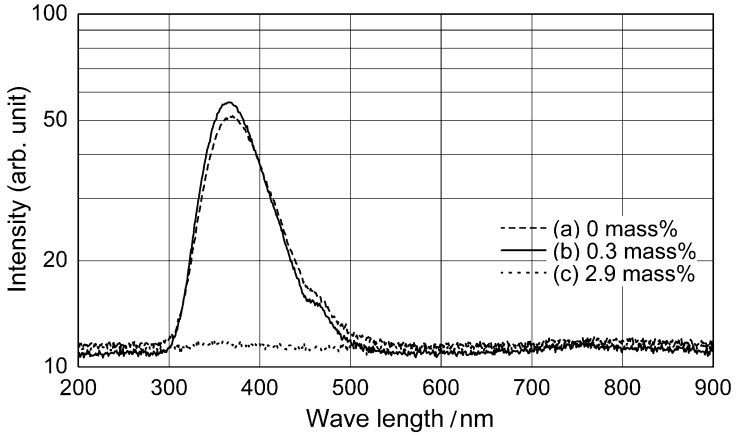

Fig. 7. Cathodoluminescence spectra of the AlN ceramics sintered at 1900°C. The Y_2O_3 amounts are (a) 0 mass%, (b) 0.3 mass% and (c) 2.9 mass% Y_2O_3.

Table 1. Summary of the Characteristics of AlN Ceramics Sintered at 1900°C

	No additive	Y_2O_3 0.3 mass%	Y_2O_3 2.9 mass%
Electrical Analysis			
Volume Resistivity (R. T., $\Omega \cdot$ cm)	5×10^{12}	1×10^{10}	6×10^{13}
Grain (R. T., $\Omega \cdot$ cm)	5×10^{8}	2×10^{8}	$>10^{13}$
Grain boundary (R. T., $\Omega \cdot$ cm)	1×10^{12}	3×10^{10}	$>10^{13}$
Thermal Conductivity (W/mK)	81	99	183
Microstructural Analysis			
Oxygen concentration, EPMA	High	High	Low
Oxygen (calculated, atom/cm^3)	10.2×10^{20}	7.8×10^{20}	2.7×10^{20}
Cathodoluminescence	370 nm, Strong	370 nm, Strong	None
XRD Analysis			
Lattice constant, c-axis (Å)	4.9783	4.9797	4.9802
Secondary phase	Al_5O_6N	Al_5O_6N, $Y_3Al_5O_{12}$	$YAlO_3$

boundaries causing the higher resistivity. Furthermore, the remarkably observed difference in the fracture morphology, where one had an intergranular fracture in majority and the other was an intergranular fracture, indicates a large microstructural difference exists at their grain boundaries. It is necessary to perform a detailed analysis at the grain boundary in order to relate the electrical property and microstructural characteristics at the boundary.

The activation energies shown in the Arrhenius plots of Fig. 2 are small in the low resistive samples and large in the high ones. It is considered that the higher concentrations of conductive carriers of low resistive samples are less sensitive to the elevated temperature so that they are leading to a smaller activation energy.

5. Conclusion

Dense AlN ceramics containing different amounts of Y_2O_3 were prepared by hot-pressing and their electrical resistivity was evaluated. Compared to the AlN without Y_2O_3, it was found that the addition of a small amount of Y_2O_3 within 0.1 to 0.5mass% remarkably decreased the electrical resistivity to 10^{10} $\Omega \cdot$cm. On the other hand, a larger amount of Y_2O_3 addition by more than 0.5 mass% increased the electrical resistivity to more than 10^{13} $\Omega \cdot$ cm, where the thermal conductivity also increased with Y_2O_3 amount. The combination of different analytical techniques performed in this study explained the mechanisms of the decrease in electrical resistivity as follows. The oxygen dissolution in the AlN grain typically observed in the sample with 0.3 mass% Y_2O_3 generates the impurity level in the bandgap of AlN, which is contributing to the increase of conductive carrier concentration in the AlN.

Reference

1) K. Komeya, *Ceramics Japan*, **26**, 725–32 (1991).
2) Y. Nagano, *Ceramics Japan*, **36**, 262–263 (2001).
3) T. Shirai and K. Miyashita, *Ceramics Japan*, **39**, 684–687 (2004).
4) T. Mizutani, T. Mizuno, R. Ushikoshi, H. Kobayashi and K. Watanabe, *FC Report*, **18**, 152–156 (2000).
5) K. Kawasaki, *Ceramics Japan*, **39**, 688–691 (2004).
6) K. Shinozaki, N. Mizutani and Y. Sawada, *FC Report*, **15**, 244–249 (1997).
7) K. Watari, *J. Ceram. Soc. Japan*, **109**, S7–S16 (2001).
8) V. L. Richards, T. Y. Tien and R. D. Pehlke, *J. Mater. Sci.*, **22**, 3385–3390 (1987).
9) M. Yahagi and K. Goto, *J. Jpn. Inst. Metals*, **47**, 419–425 (1983).
10) W. A. Groen and P. F. van Hal, *British Ceramic Transaction*, **93**, 192–195 (1994).
11) J. Yoshikawa, Y. Katsuda, N. Yamada, C. Ihara, M. Masuda and H. Sakai, *J. Am. Ceram. Soc.*, **88**, 3501–3506 (2005).
12) E. M. Levin and H. F. McMurdie, "Phase Diagrams for Ceramists", Ed. by M. K. Reser, The American Ceramic Society, Ohio (1975) 132, Fig. 4370.
13) G. A. Slack, *J. Phys. Chem. Solids*, **34**, 321–35 (1973).